

Recovery of optical parameters in multiple-layered diffusive media: theory and experiments

Jorge Ripoll

Instituto de Ciencia de Materiales de Madrid, Consejo Superior de Investigaciones Científicas, Campus de Cantoblanco, 28049 Madrid, Spain

Vasilis Ntziachristos

Department of Biochemistry/Biophysics, University of Pennsylvania, Philadelphia, Pennsylvania 19104-6089

Joe P. Culver, Deva N. Pattanayak, and Arjun G. Yodh

Department of Physics and Astronomy, University of Pennsylvania, Philadelphia, Pennsylvania 19104-6089

Manuel Nieto-Vesperinas

Instituto de Ciencia de Materiales de Madrid, Consejo Superior de Investigaciones Científicas, Campus de Cantoblanco, 28049 Madrid, Spain

Received March 30, 2000; revised manuscript received October 4, 2000; accepted October 18, 2000.

Diffuse photon density waves have lately been used both to characterize diffusive media and to locate and characterize hidden objects, such as tumors, in soft tissue. In practice, most biological media of medical interest consist of various layers with different optical properties, such as the fat layer in the breast or the different layers present in the skin. Also, most experimental setups consist of a multilayered system, where the medium to be characterized (i.e., the patient's organ) is usually bounded by optically diffusive plates. Incorrect modeling of interfaces may induce errors comparable to the weak signals obtained from tumors embedded deep in highly heterogeneous tissue and lead to significant reconstruction artifacts. To provide a means to analyze the data acquired in these configurations, the basic expressions for the reflection and transmission coefficients for diffusive–diffusive and diffusive–nondiffusive interfaces are presented. A comparison is made between a diffusive slab and an ordinary dielectric slab, thus establishing the limiting distance between the two interfaces of the slab for multiple reflections between them to be considered important. A rigorous formulation for multiple-layered (M -layered) diffusive media is put forward, and a method for solving any M -layered medium is shown. The theory presented is used to characterize a two-layered medium from transmission measurements, showing that the coefficients of scattering, μ'_s , and absorption, μ_a , are retrieved with great accuracy. Finally, we demonstrate the simultaneous retrieval of both μ'_s and μ_a . © 2001 Optical Society of America

OCIS codes: 170.5270, 290.1990, 290.7050.

1. INTRODUCTION

Diffuse photon-density waves (DPDW's) are scalar-damped traveling disturbances of light energy propagating in turbid media from an oscillating source. The present interest on them stems from their potential to locate objects hidden within these highly scattering media. The diffusion approximation¹ has been shown to be reasonably good in many practical situations for describing light transport.^{2,3} Light propagating within the diffusion approximation has been investigated for determining the scattering and absorption coefficients of biological media as well as for formulating medical diagnoses.^{3–9} So far, several experiments have been performed in this area, with encouraging results,¹⁰ and basic concepts of wave propagation such as Snell's law or diffraction from an edge have been experimentally verified.^{11,12} One important area in this field is the study of multiple-layered dif-

usive media,^{13–23} which has been focused mainly on reflection measurements from the skin. However, reflection measurements are not sensitive to small objects embedded deep into tissue (~ 3 cm) in which case transmission measurements must also be performed. Recently, the expressions for the reflection and transmission coefficients have been presented in the case of diffusive–diffusive interfaces.²⁴ However, other basic properties that govern these waves have not yet been established. These pertain to the reflection and refraction coefficients of their plane-wave components at the interface between a diffusive medium and an outer nondiffusive medium, where detection is performed, and to the use of these coefficients in solving multiple-layered media. This is of importance for straightforwardly determining the optical parameters. Also, these properties give us the exact value of the Green's function in any of the layers, thus en-

abling us to improve the accuracy of hidden-object reconstruction within such systems. In many experimental configurations, the medium to be characterized is usually bounded between two diffusive plates. Hence, it is quite common to have a diffusive–diffusive interface between the plate and the medium and a diffusive–nondiffusive interface at the output. In most cases, to detect and characterize a hidden object within such media, this system is approximated as a one-layered medium or as a semi-infinite homogeneous medium. With the aid of the reflection and transmission coefficients for diffusive–diffusive interfaces, however, multiple-layered (M -layered) configurations in contact with nondiffusive media can be analytically solved in terms of these coefficients, thus speeding up the computation time.

In Section 2 we establish the expressions for the reflection and transmission coefficients of DPDW plane-wave components between a diffusive and a nondiffusive medium, discussing in Section 3 how an M -layered medium can be exactly solved. We consider the case of a single slab and how it compares with a dielectric slab, a consequence being that devising resonator interferometers²⁵ is not possible for DPDW's. In Section 4 we present the experimental setup used to verify our theory, and we present the procedure employed to fit the data in Section 5. The experimental results and simulations obtained from two different expressions for the transmitted wave, namely, a two-layered and a one-layered medium, are shown in Section 6, where we demonstrate that the two-layer expression yields accurate values of both μ_a and μ'_s , whereas the one-layer, or semi-infinite, expressions fail to do so. In this manner, we establish a straightforward, novel, and systematic procedure for characterizing diffusive media by means of these reflection and transmission coefficients on measurements performed from a nondiffusive exterior medium. Finally, in Section 7 we present the summary and conclusions.

2. REFLECTION AND TRANSMISSION COEFFICIENTS

An infinite homogeneous diffusive medium is characterized by its absorption coefficient μ_a , the refractive index n , and the diffusion coefficient $D = 1/[3\mu'_s]$, where μ'_s is the reduced scattering coefficient. For an intensity-modulated source at a frequency ω , the average intensity $U(\mathbf{r}, t) = U(\mathbf{r})\exp(-i\omega t)$ represents the DPDW and obeys the Helmholtz equation with a wave number $\kappa_0 = [-\mu_a/D + i\omega/(vD)]^{1/2}$, where $v = c/n$ is the speed of light in the medium. Let a source or object be at a plane $z = z_s$. At any plane $z = \text{constant}$ of a homogeneous diffusive half-space, we can express the average intensity $U(\mathbf{r})$ by its angular-spectrum representation of plane waves, that is, by a superposition of waves of amplitude $\mathcal{A}(\mathbf{K})$ and wave vector $\mathbf{k} = (\mathbf{K}, q)$, $|\mathbf{k}| = \kappa_0$ [Refs. 26–29]:

$$(U\mathbf{R}, z) = \int_{-\infty}^{+\infty} \mathcal{A}(\mathbf{K})\exp[i\mathbf{K} \cdot \mathbf{R} + iq(\mathbf{K})|z - z_s|]d\mathbf{K}, \quad (1)$$

where $|\mathbf{K}|^2 + q^2 = \kappa_0^2$; i.e., $\mathbf{K} = (K_x, K_y)$ is a real vector and $q(\mathbf{K}) = (\kappa_0^2 - |\mathbf{K}|^2)^{1/2}$. For DPDW's, since κ_0 is always a complex number, $q(\mathbf{K}) = q_{\text{re}} + iq_{\text{im}}$ is always

complex, namely, $q_{\text{im}} \neq 0$. In Eq. (1), we choose $q_{\text{re}} > 0$ and $q_{\text{im}} > 0$ so that the field satisfies the radiation condition at infinity. From Eq. (1), we also obtain the relationships

$$U(\mathbf{K}, z) = \mathcal{A}(\mathbf{K})\exp[iq(\mathbf{K})|z - z_s|], \quad (2)$$

$$\tilde{J}_n(\mathbf{K}, z) = -D \frac{\partial \tilde{U}(\mathbf{K}, z)}{\partial z} = -iDq(\mathbf{K})\tilde{U}(\mathbf{K}, z), \quad (3)$$

where $\tilde{U}(\mathbf{K}, z)$ is the Fourier transform of $U(\mathbf{R}, z)$. In Eq. (3), $\tilde{J}_n(\mathbf{K}, z)$ is the Fourier transform of the total flux density at plane z , $J_n(\mathbf{R}, z)$, and is Fick's law in the angular-spectrum representation.

A. Diffusive–Nondiffusive Interfaces

We shall now derive the reflection and transmission coefficients between diffusive and nondiffusive media. The expressions for diffusive–diffusive interfaces can be found in Ref. 24. Let us consider an isotropic and homogeneous semi-infinite diffusive medium ($z > 0$), separated by a plane interface at $z = 0$ from a nondiffusive semi-infinite half-space ($z < 0$). The upper diffusive medium is characterized by D_0 , μ_{a0} , n_0 , and κ_0 , and the lower medium is characterized by n_1 . Let the light source be located at $z_s > 0$, with the total wave represented by $U_0 = U^{(i)} + U^{(r)}$, and $U_1 = U^{(t)}$ in the upper and lower media, respectively. The expression for $U^{(t)}$ is valid only at the interface, since propagation into the nondiffusive medium cannot be described by the diffusion approximation (see Ref. 30 for a detailed description of this problem). To find the relationship between $U^{(i)}$, $U^{(r)}$, and $U^{(t)}$ across the interface, and hence the expressions for the reflection and transmission coefficients \mathcal{R}_{nd} and \mathcal{T}_{nd} , we must apply the saltus condition at $z = 0$. In the diffusion approximation context, this condition is expressed by the zero flux requirement, which states that the total flux J_n traversing the interface is an outward flux J_+ , i.e., the inward flux J_- is zero,^{31,32} and therefore $\mathbf{J}(\mathbf{r}) \cdot \hat{\mathbf{n}} = J_n(\mathbf{r}) = J_+(\mathbf{r})$. This is to be expected if there are no other light sources in the outer nondiffusive medium that could generate an inward flux. The zero-flux condition is expressed in terms of the average intensity U_0 as

$$U_0(\mathbf{R}, z)|_{z=0} = \alpha J_n(\mathbf{R}, z)|_{z=0} = -D_0\alpha \left. \frac{\partial U_0(\mathbf{R}, z)}{\partial z} \right|_{z=0}, \quad (4)$$

where α is a coefficient that takes into account refractive-index mismatch, with the quantity $D_0\alpha = l_{\text{tr}}\alpha/3$ usually referred to as the extrapolated distance,^{1,31,32} where l_{tr} is the transport mean free path. In Eq. (4) we have taken the surface unit normal $\hat{\mathbf{n}} = \hat{\mathbf{u}}_z$ to be pointing outward, i.e., into the nondiffusive medium [when the surface normal is considered pointing inward, α in Eq. (4) must be replaced by $-\alpha$]. Substituting Eq. (3) into Eq. (4), we obtain

$$\tilde{U}^{(i)}(\mathbf{K}, z = 0) + \tilde{U}^{(r)}(\mathbf{K}, z = 0) = \alpha \tilde{J}_n(\mathbf{K}, z = 0), \quad (5)$$

$$\begin{aligned} \tilde{J}_n(\mathbf{K}, z = 0) &= -D_0[iq(\mathbf{K})\tilde{U}^{(i)}(\mathbf{K}, z = 0) \\ &\quad - iq(\mathbf{K})\tilde{U}^{(r)}(\mathbf{K}, z = 0)], \end{aligned} \quad (6)$$

where Eq. (6) represents Fick's law and takes into account the opposite-propagation directions of $U^{(i)}$ and $U^{(r)}$. After some simple algebra, by means of Eq. (2), Eqs. (5) and (6) reduce to

$$\mathcal{A}^{(r)}(\mathbf{K}) = \mathcal{R}_{\text{nd}}(\mathbf{K})\tilde{U}^{(i)}(\mathbf{K}, z = 0), \quad (7)$$

$$J_n(\mathbf{K}, z = 0) = \frac{1}{\alpha} \mathcal{T}_{\text{nd}}(\mathbf{K})\tilde{U}^{(i)}(\mathbf{K}, z = 0), \quad (8)$$

where

$$\mathcal{R}_{\text{nd}}(\mathbf{K}) = \frac{i\alpha D_0 q(\mathbf{K}) + 1}{i\alpha D_0 q(\mathbf{K}) - 1}, \quad (9)$$

$$\mathcal{T}_{\text{nd}}(\mathbf{K}) = \frac{2i\alpha D_0 q(\mathbf{K})}{i\alpha D_0 q(\mathbf{K}) - 1}, \quad (10)$$

\mathcal{R}_{nd} and \mathcal{T}_{nd} being the frequency-dependent reflection and transmission coefficients, respectively, for diffusive–nondiffusive interfaces. Both \mathcal{R}_{nd} and \mathcal{T}_{nd} are complex, and the sum of their moduli is not unity, but they hold the relationship $\mathcal{T}_{\text{nd}}(\mathbf{K}) = \mathcal{R}_{\text{nd}}(\mathbf{K}) + 1$. As can be seen in Eq. (8), we have expressed the transmission coefficient in terms of the total density flux that traverses the interface. The reason for this is that when measurements are performed from an outer nondiffusive medium, usually the measured quantity is J_n , through Lambert's cosine law^{25,30} and not $U^{(t)}$. In any case, the value of $U^{(t)}$ can be directly obtained from Eq. (4), and therefore

$$\tilde{U}^{(t)}(\mathbf{K}, z = 0) = \mathcal{T}_{\text{nd}}(\mathbf{K})\tilde{U}^{(i)}(\mathbf{K}, z = 0). \quad (11)$$

Black Interface. With a particular case of diffusive–nondiffusive interface, we consider that in which the lower medium is perfectly absorbing, i.e., a black slab. The boundary condition at such an interface is

$$U_0(\mathbf{R}, z)|_{z=0} = U^{(i)}(\mathbf{R}, z)|_{z=0} + U^{(r)}(\mathbf{R}, z)|_{z=0} = 0, \quad (12)$$

which results in the following reflection and transmission coefficients for diffusive–black interfaces:

$$\mathcal{R}_{\text{black}}(\mathbf{K}) = -1, \quad (13)$$

$$\mathcal{T}_{\text{black}}(\mathbf{K}) = 0. \quad (14)$$

This relationship is what is expected from Eq. (12), since absorption is simply scattering with a π dephase, i.e., $U^{(r)}(\mathbf{R}, z = 0) = U^{(i)}(\mathbf{R}, z = 0)\exp[i\pi]$, and in the case of a perfect absorber, with the property $|U^{(r)}| = |U^{(i)}|$. Eqs. (13) and (14) are equivalent to introducing $\alpha = 0$ into \mathcal{T}_{nd} and \mathcal{R}_{nd} [see Eq. (4)].

B. Incident Field

To solve any multiple-layered configuration, we need an expression for the incident field, i.e., for its angular-spectrum representation. This can be obtained for a source located at z_s by means of Eq. (1), namely,

$$\mathcal{A}^{(i)}(\mathbf{K}) = \frac{1}{4\pi^2} \int_{-\infty}^{+\infty} U^{(i)}(\mathbf{R}, z = z_s) \exp[-i\mathbf{K} \cdot \mathbf{R}] d\mathbf{R}. \quad (15)$$

In the case of a point source $U^{(i)}(\mathbf{R}, z = z_s) = S_0 \exp[i\kappa_0 R]/(4\pi D_0 R)$, Eq. (15) reduces to (see Refs. 27, 33 for a detailed derivation)

$$\mathcal{A}^{(i)}(\mathbf{K}) = \frac{S_0}{4\pi D_0} \frac{i}{2\pi q(\mathbf{K})}, \quad (16)$$

where S_0 is the source strength. Substituting Eq. (16) into Eq. (1) yields the Weyl representation of a diverging spherical wave,^{27,28} which is a very useful tool for localizing and characterizing hidden objects in diffusive media.^{34,35} By means of Eq. (2), the expression for a point source at any plane z is

$$\tilde{U}^{(i)}(\mathbf{K}, z) = \frac{S_0}{4\pi D_0} \frac{i}{2\pi q_i(\mathbf{K})} \exp[iq_i(\mathbf{K})|z - z_s|]. \quad (17)$$

The incident field measured at a plane $z \leq 0$, due to a point source located at distance z_s from a black boundary, is [see Eqs. (13) and (17)]

$$\begin{aligned} \tilde{U}^{(i)}(\mathbf{K}, z) = \frac{S_0}{4\pi D_0} \frac{i}{2\pi q_i(\mathbf{K})} \{ & \exp[iq_i(\mathbf{K})|z - z_s|] \\ & - \exp[iq_i(\mathbf{K})|z + z_s|] \}. \end{aligned} \quad (18)$$

For $z > z_s$, Eq. (18) can be rewritten as

$$\tilde{U}^{(i)}(\mathbf{K}, z) = \frac{S_0}{4\pi^2 D_0} \frac{\exp[iq_i(\mathbf{K})z]}{q_i(\mathbf{K})} \sinh[iq_i(\mathbf{K})z_s]. \quad (19)$$

We should state that the correct way to represent the source is to include an angular-dependent, or dipolar, term as in Ref. 36. Nevertheless, since this effect decays at long distances from the source, we will from now on use Eqs. (17) and (18) to model the incident field.

3. MULTIPLE-LAYERED MEDIA

We next solve any multiple-layered (M -layered) system without any approximation. For the sake of clarity, we shall first address the simple system consisting of a slab that is equivalent to a three-layered medium. This is done for two reasons: First, the expression for a slab will be very useful, since in many cases, a system of multiple layers can be approximated by a system of slabs with no multiple reflections between them; second, a great deal of information, such as the limiting depth at which information from an object can be recovered or the multiple-reflection contribution, can be extracted.

A. Expression for a Slab

Let us address the configuration depicted in Fig. 1, namely, a slab of width L , located at $0 < z < L$. At $z > L$ there is a semi-infinite homogeneous medium of parameters D_0 , μ_{a0} , n_0 , and κ_0 , with a source located at z_s . At $z < 0$ we have a semi-infinite homogeneous medium of parameters D_2 , μ_{a2} , n_2 , and κ_2 . The slab has D_1 , μ_{a1} , n_1 , and κ_1 as parameters. We shall consider the normal $\hat{\mathbf{n}}$ at the interfaces to be pointing in the $-z$ direction, i.e., $\hat{\mathbf{n}} = (0, 0, -1)$. There are two ways of solving this configuration. The first method consists of introducing the boundary conditions at each of the interfaces and solving the linear system of equations by following a

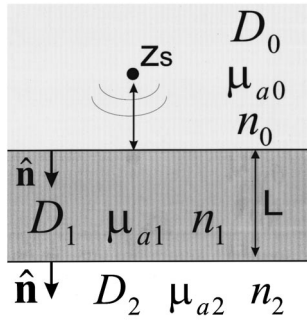


Fig. 1. Configuration for a slab where three different zones are distinguished, with different diffusive parameters: $z \geq L$, $0 \leq z \leq L$, and $z \leq 0$.

scheme similar to that presented in Refs. 15, 17, 19, and 23 for a two-layered medium. This is the method that will be employed for solving M -layered systems. The second method consists of successively adding multiple reflections and transmissions at the interfaces, and since it is physically illustrative we shall use it to derive the expressions for a slab.

The total wave in the three regions of Fig. 1 is $\tilde{U}^{(i)} + \mathcal{A} \exp[iq_0(z - L)]$, $z > L$; $\mathcal{B} \exp[iq_1(L - z)] + \mathcal{C} \exp[iq_1z]$, $L > z > 0$; and $\mathcal{D} \exp[-iq_2z]$, $z < 0$. Considering all multiple reflections from the interfaces, the total reflection and transmission coefficients for the slab are^{25,37}

$$\begin{aligned} \mathcal{R}^{\text{slab}} &= \mathcal{R}_{01} + \mathcal{T}_{01} \mathcal{R}_{12} \exp[2iq_1L] \mathcal{T}_{10} + \mathcal{T}_{01} \mathcal{R}_{12} \\ &\quad \times \exp[2iq_1L] \mathcal{R}_{10} \mathcal{R}_{12} \\ &\quad \times \exp[2iq_1L] \mathcal{T}_{10} + \dots, \end{aligned} \quad (20)$$

$$\begin{aligned} \mathcal{T}^{\text{slab}} &= \mathcal{T}_{01} \exp[iq_1L] \mathcal{T}_{10} + \mathcal{T}_{01} \mathcal{R}_{12} \exp[2iq_1L] \mathcal{R}_{10} \\ &\quad \times \exp[iq_1L] \mathcal{T}_{10} + \dots, \end{aligned} \quad (21)$$

where \mathcal{R}_{ij} and \mathcal{T}_{ij} are the reflection and transmission coefficients going from medium i to medium j (Ref. 24). Equations (20) and (21) contain a geometric progression, and therefore \mathcal{A} , \mathcal{B} , \mathcal{C} , and \mathcal{D} are extracted as

$$\begin{aligned} \mathcal{A} &= \left\{ \mathcal{R}_{01} + \frac{\mathcal{T}_{01} \exp[2iq_1L] \mathcal{R}_{12} \mathcal{T}_{10}}{1 - \mathcal{R}_{10} \mathcal{R}_{12} \exp[2iq_1L]} \right\} \tilde{U}^{(i)}, \\ \mathcal{B} &= \frac{\mathcal{T}_{01}}{1 - \mathcal{R}_{10} \mathcal{R}_{12} \exp[2iq_1L]} \tilde{U}^{(i)}, \\ \mathcal{C} &= \frac{\mathcal{T}_{01} \exp[iq_1L] \mathcal{R}_{12}}{1 - \mathcal{R}_{10} \mathcal{R}_{12} \exp[2iq_1L]} \tilde{U}^{(i)}, \\ \mathcal{D} &= \frac{\mathcal{T}_{01} \exp[iq_1L] \mathcal{T}_{12}}{1 - \mathcal{R}_{10} \mathcal{R}_{12} \exp[2iq_1L]} \tilde{U}^{(i)}. \end{aligned} \quad (22)$$

From Eqs. (22) the reflection and transmission coefficients for a slab are defined as

$$\mathcal{R}^{\text{slab}}(\mathbf{K}) = \mathcal{R}_{01} + \frac{\mathcal{T}_{01} \exp[2iq_1L] \mathcal{R}_{12} \mathcal{T}_{10}}{1 - \mathcal{R}_{10} \mathcal{R}_{12} \exp[2iq_1L]}, \quad (23)$$

$$\mathcal{T}^{\text{slab}}(\mathbf{K}) = \frac{\mathcal{T}_{01} \exp[iq_1L] \mathcal{T}_{12}}{1 - \mathcal{R}_{10} \mathcal{R}_{12} \exp[2iq_1L]}. \quad (24)$$

Equations (23) and (24) correspond to a dielectric slab.²⁵ For a gain medium, they represent the equations for a Fabry–Perot laser cavity,³⁷ and $\mathcal{R}_{10} \mathcal{R}_{12} \exp[2iq_1L] = 1$ represents the oscillation condition. In Eqs. (23) and (24), the denominator $1 - \mathcal{R}_{10} \mathcal{R}_{12} \exp[2iq_1L]$ takes into account the multiple reflections between the interfaces of the slab. Since in general for DPDW's $\mathcal{R}_{10} \mathcal{R}_{12} \exp[2iq_1L] \ll 1$, the geometric progression can be truncated to first order, i.e.,

$$\mathcal{R}^{\text{slab}} \approx \mathcal{R}_{01} + \mathcal{T}_{01} \exp[2iq_1L] \mathcal{R}_{12} \mathcal{T}_{10},$$

$$\mathcal{T}^{\text{slab}} \approx \mathcal{T}_{01} \exp[iq_1L] \mathcal{T}_{12}.$$

These approximations are very accurate, even for low values of L , as shown in Fig. 2. In this figure one sees that for values of L greater than 3 cm the reflection from the slab is simply \mathcal{R}_{01} . Therefore $\mathcal{R}_{10} \mathcal{R}_{12} \exp[2iq_1L]$ represents a way of determining the distance at which multiple reflections between the walls are important. As a rule of thumb, we can use the following criterion: Assuming 0.1% noise in the measurements, the limiting value of $\exp[2iq_1L]$ for absence of multiple reflection is 0.1% at best. This means $L = -\log[10^{-3}]/2\kappa_0$ for the case $\omega = 0$, $\mathbf{K} = 0$. Therefore the limiting value of L is approximately

$$L_{\text{limit}} \sim 3(D_1/\mu_{a1})^{1/2}. \quad (25)$$

For example, in Fig. 2, for $\mu'_{s1} = 10 \text{ cm}^{-1}$ we show that $L_{\text{limit}} \sim 3 \text{ cm}$, and for $\mu'_{s1} = 20 \text{ cm}^{-1}$, we obtain $L_{\text{limit}} \sim 2.5 \text{ cm}$.

For a dielectric slab, the condition $\mathcal{R}_{10} \mathcal{R}_{12} \exp[2iq_1L] \sim 1$ conveys the existence of transmission and reflection

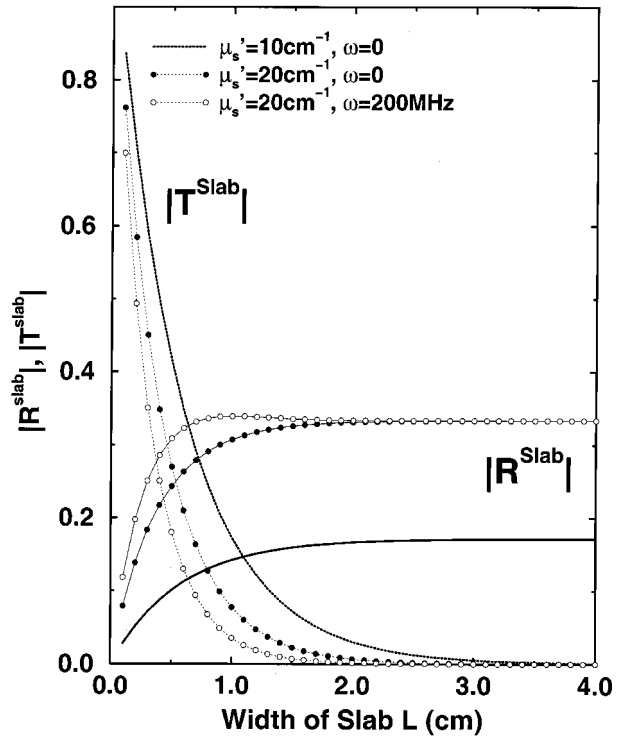


Fig. 2. Amplitude of $\mathcal{R}^{\text{slab}}$ and $\mathcal{T}^{\text{slab}}$ at $\mathbf{K} = 0$ for different values of the slab width L for the cases $\mu'_{s1} = 10 \text{ cm}^{-1}$, $\omega = 0$ (solid curves); $\mu'_{s1} = 20 \text{ cm}^{-1}$, $\omega = 0$ (solid circles); $\mu'_{s1} = 20 \text{ cm}^{-1}$, $\omega = 200 \text{ MHz}$ (open circles). In all cases $\mu'_{s0} = \mu'_{s2} = 5 \text{ cm}^{-1}$, $\mu_{a0} = \mu_{a1} = \mu_{a2} = 0.025 \text{ cm}^{-1}$, $n_0 = n_1 = n_2 = 1.333$.

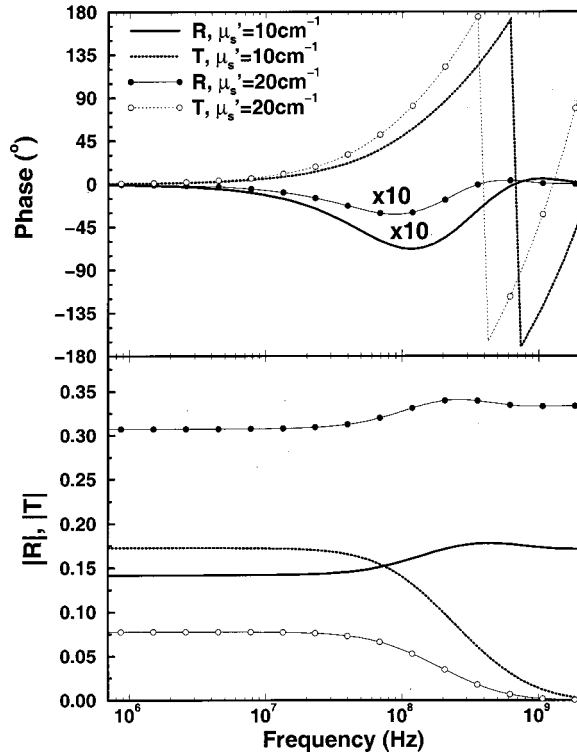


Fig. 3. Amplitude and phase of $\mathcal{R}^{\text{slab}}$ and $\mathcal{T}^{\text{slab}}$ at $\mathbf{K} = 0$ for different values of the modulation frequency ω for the cases $\mu_{s1}' = 10 \text{ cm}^{-1}$ [$\mathcal{R}^{\text{slab}}$ (solid curves) and $\mathcal{T}^{\text{slab}}$ (dotted curves)], $\mu_{s1}' = 20 \text{ cm}^{-1}$ [$\mathcal{R}^{\text{slab}}$ (solid circles) and $\mathcal{T}^{\text{slab}}$ (open circles)]. In all cases $\mu_{s0}' = \mu_{s2}' = 5 \text{ cm}^{-1}$, $\mu_{a0} = \mu_{a1} = \mu_{a2} = 0.025 \text{ cm}^{-1}$, $n_0 = n_1 = n_2 = 1.333$.

resonant peaks. However, this requires values of \mathcal{R}_{10} and \mathcal{R}_{12} close to unity. This is not the case for a diffusive

$$[\hat{M}] \equiv \begin{bmatrix} f_{\text{in}} & -g_{\text{in}}E_1 & 0 & 0 & 0 & 0 & \cdots & 0 & 0 \\ a_{12}E_1 & b_{12} & -1 & -E_2 & 0 & 0 & \cdots & 0 & 0 \\ q_1D_1E_1 & -q_1D_1 & -q_2D_2 & q_2D_2E_2 & 0 & 0 & \cdots & 0 & 0 \\ 0 & 0 & a_{23}E_2 & b_{23} & -1 & -E_3 & \cdots & 0 & 0 \\ 0 & 0 & q_2D_2E_2 & -q_2D_2 & -q_3D_3 & q_3D_3E_3 & \cdots & 0 & 0 \\ \vdots & \vdots & \vdots & \vdots & \vdots & \vdots & \ddots & \vdots & \vdots \\ 0 & 0 & 0 & 0 & 0 & 0 & \cdots & -q_M D_M & q_M D_M E_M \\ 0 & 0 & 0 & 0 & 0 & 0 & \cdots & -g_{\text{out}}E_M & f_{\text{out}} \end{bmatrix}, \quad (28)$$

slab. Also, we must take into consideration that q_1 is always complex, and therefore $\exp[iq_1L]$ represents a lossy medium as it decays with L . The behavior of $\mathcal{R}^{\text{slab}}$ and $\mathcal{T}^{\text{slab}}$ versus the modulation frequency $f = \omega/2\pi$ is shown in Fig. 3, where we see that for $f < 1$ MHz very little difference is observed in the dc ($\omega = 0$) case. For high values of ω , we must recall that the imaginary part of q_1 , and therefore the decay of $\exp[2iq_1L]$, grows as $\omega^{1/2}$. Nevertheless, in Fig. 3 we distinguish maxima near $f = 200$ MHz. These maxima correspond to maximum values of $\exp[2iq_1L]$ and therefore cannot be considered as resonant peaks as for the dielectric slab. We therefore

conclude that Fabry–Perot resonators are not possible for DPDWs. Additional useful information contained in Eq. (23) pertains to the maximum distance between the slab walls from which parameters from medium 2 can be extracted when reflection measurements from medium 0 are performed, since all the information from medium 2 is contained in $\mathcal{R}_{12} \exp[2iq_1L]$. In this case we can also use Eq. (25), thus concluding that in reflection measurements, it is not possible to characterize an object buried at a distance larger than L_{limit} from the first interface. By contrast, as seen from Eq. (24), this does not occur in transmission measurements, since information of all the media is present in the wave field.

B. Solving Multiple-Layered Media

Let us address an M -layered system, as depicted in Fig. 4, where n_{in} corresponds to the refractive index of the non-scattering medium that bounds the medium containing the source and n_{out} stands for the refractive index of the non-scattering medium where detection is performed. An equivalent solution for multiple-layered dielectric media can be found in Ref. 25. In any of the j th inner media, the total field for each frequency component is

$$U_j = A_j \exp[iq_j(z_j - z)] + B_j \exp[iq_j(z - z_{j+1})], \quad z_j \leq z \leq z_{j+1}, \quad (26)$$

where z_j is the position of j th interface, i.e., $z_j = \sum_{k=1}^{j-1} L_k$, L_k being the width of medium k . On introducing the saltus conditions for each of the interfaces, taking into consideration that the first and last interfaces are diffusive–nondiffusive, we get to the following set of equations:

$$[\hat{M}]_{M \times M} \cdot [\hat{X}]_{M \times 1} = [\hat{Y}]_{M \times 1}, \quad (27)$$

where

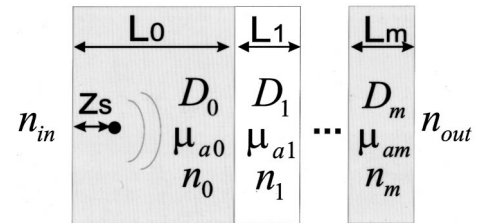


Fig. 4. Multiple-layered configuration of M slabs, where n_{in} and n_{out} are the refractive indices of the input and output media, respectively, with both being nondiffusive. In all cases, the normal to each interface is considered to point from n_{in} into n_{out} , i.e., along the propagation direction of the incident wave.

$$[\hat{X}] \equiv \begin{pmatrix} \mathcal{A}_1 \\ \mathcal{B}_1 \\ \vdots \\ \mathcal{A}_M \\ \mathcal{B}_M \end{pmatrix}; \quad [\hat{Y}] \equiv \begin{pmatrix} g_{\text{in}} \tilde{U}^{(i)}(\mathbf{K}, z=0) \\ -a_{12} \tilde{U}^{(i)}(\mathbf{K}, z=0) \\ 0 \\ \vdots \\ 0 \end{pmatrix}, \quad (29)$$

and

$$E_j = \exp[iq_j L_j], \quad (30)$$

$$a_{jk} = (n_k/n_j)^2 + iC_{jk} D_j q_j, \quad (31)$$

$$b_{jk} = (n_k/n_j)^2 - iC_{jk} D_j q_j. \quad (31)$$

Equations (31) are the coefficients for the boundary conditions between the j th and $k = j + 1$ diffusive media, which in the case $n_j = n_k$ have the values $a_{jk} = b_{jk} = 1$ (see Refs. 24, 38). For the input and output interfaces we have defined

$$f_{\text{in}} = i\alpha_{\text{in}} q_1 D_1 - 1; \quad g_{\text{in}} = i\alpha_{\text{in}} q_1 D_1 + 1, \quad (32)$$

$$f_{\text{out}} = i\alpha_{\text{out}} q_M D_M - 1; \quad g_{\text{out}} = i\alpha_{\text{out}} q_M D_M + 1, \quad (33)$$

which when the input interface is black ($\alpha_{\text{in}} = 0$), yield $f_{\text{in}} = -1$, $g_{\text{in}} = 1$. Notice that $g_x/f_x = \mathcal{R}_{\text{nd}}$ [see Eq. (9)]. As seen from Eq. (27), after solving the linear system of equations we are left with an $M \times 1$ matrix that represents the values of \mathcal{A}_j , \mathcal{B}_j for each frequency component. That is, Eq. (27) must be solved for each frequency component. Once these \mathcal{A}_j , \mathcal{B}_j coefficients are found, the total field can be built inside any of the slabs by Eq. (26).

4. EXPERIMENTAL SETUP

To test the theory, we measured a two-layer system composed of an intralipid layer and a resin layer, as depicted in Fig. 5. This setup is one that can be used to perform breast measurements in the cw regime, i.e., no modulation frequency, in which case the breast is introduced in intralipid. The resin was a polyester resin with a TiO₂ suspension³⁹ of length $L_1 = 2.17$ cm with optical parameters $\mu'_{s1} = 10$ cm⁻¹, $\mu_{a1} = 0.017$ cm⁻¹, and $n_1 = 1.5$. The intralipid used was an Intralipid (Kabi Pharmacia, Clayton, North Carolina) emulsion, which is a polydisperse suspension of fat particles ranging in diameter from 0.1 to 1.1 μm that served as the scattering background medium. This intralipid layer had a length $L_0 = 4$ cm and parameters μ'_{s0} , μ_{a0} , and n_0 , for which three different values of μ'_{s0} , were used, namely, $\mu_{s0}^{(i=1,2,3)} = 5$ cm⁻¹, 10 cm⁻¹, and 20 cm⁻¹. For each of these sets $\mu_{s0}^{(i)}$, five values of μ_{a0} were introduced, namely, $\mu_{a0}^{(j=1,\dots,5)} = 0.025$ cm⁻¹, 0.050 cm⁻¹, 0.075 cm⁻¹, 0.1 cm⁻¹, and 0.125 cm⁻¹, constituting a total of 15 different $\mu_{s0}^{(i)}$, $\mu_{a0}^{(j)}$ pairs. In all cases the refractive index of the intralipid was $n_0 = 1.333$. To carry out the experiment, the necessary amount of intralipid was mixed with water to obtain the value of μ'_{s0} desired. Then the value of μ_{a0} was changed by introducing black India ink (3080-4 KOH-I-NOOR Inc., Bloomsbury, New York) into the mixture, performing a measurement for each $\mu_{s0}^{(i)}$, $\mu_{a0}^{(j)}$ pair.

As shown in Fig. 5, the system had side walls of black PVC. Measurements were performed at the exit of the

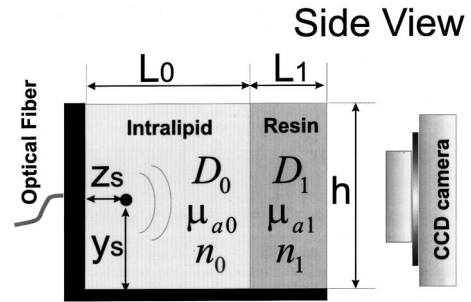


Fig. 5. Experimental setup.

resin layer. This means that the configuration had three interfaces, namely, black–intralipid, intralipid–resin, and resin–air interfaces. The basin had a height $h = 15$ cm, width $w = 25$ cm, and total length $L = 7$ cm (including the black PVC walls). In spite of the finite size of the basin, we consider the system to be infinite in the XY plane, and thus the expressions put forward in Section 2 will be employed. Illumination was accomplished by using an optical fiber of NA = 0.36, which emitted light of constant intensity at $\lambda = 786$ nm with a laser diode power ~ 3 mW, located at the rear of the basin at $(x_s = 8.6$ cm, $y_s = 8.2$ cm, $z_s = 0)$. We shall model this source by a point source located at $\mathbf{r}_s = (x_s, y_s, z_s = l_{\text{tr}})$, in the cw regime, i.e., $\omega = 0$ (constant illumination).

Measurements were taken with a liquid-nitrogen-cooled, 16-bit CCD array (Princeton Instruments), which had a resolution of 330×1100 pixels that were $24 \mu\text{m}$ in linear dimension, each pixel representing an area $dx \times dy = 0.0287$ cm \times 0.0287 cm. The CCD was focused by means of lenses on the exit surface of the resin, i.e., at $z = L_0 + L_1 = 6.17$ cm.

5. DATA ANALYSIS

The two-layered system shown in Fig. 5 is numerically solved by using Eqs. (27)–(29), with $\alpha_{\text{in}} = 0$, and $\alpha_{\text{out}} \approx 7.25$, corresponding to $n_{\text{out}} = 1$, $n_1 = 1.5$. The three interfaces of the experimental setup (see Fig. 5), two of which are diffusive–nondiffusive, yield a linear system of four equations and four unknowns. An approximation to the system of Eqs. (27)–(29) can be introduced by using Eq. (25), since we expect no contribution from multiple reflections between the walls of the intralipid, where $L_0 = 4$ cm. Also, the highest value of L_{limit} is $L_{\text{limit}} \sim 5$ cm, for the $(\mu_{s0} = 5$ cm⁻¹, $\mu_{a0} = 0.025$ cm⁻¹) case, taking into consideration that one of the interfaces is black. Hence we simply assume an incident wave coming from the intralipid whose wave function is represented by Eq. (19), which interacts with a slab (i.e., the resin block), as described by Eq. (24). Therefore, with Eq. (11), the expected average intensity at the exit of the resin, $z_d = L_0 + L_1 = 6.17$ cm, is

$$\tilde{U}_{\text{2layer}}(\mathbf{K}, z_d) = \frac{S_0}{4\pi^2 D_0} \frac{\exp[iq_0(\mathbf{K})L_0]}{q_0(\mathbf{K})} \times \sinh[iq_0(\mathbf{K})z_s] T_{\text{resin}}^{\text{slab}}(\mathbf{K}), \quad (34)$$

where $\mathcal{T}_{\text{resin}}^{\text{slab}}$ is given by Eq. (24) if medium 2 is replaced by a nonscattering medium, i.e., by replacing \mathcal{R}_{12} with \mathcal{R}_{nd} , and \mathcal{T}_{12} with \mathcal{T}_{nd} [see Eqs. (9) and (10)]. We remark that Eq. (34) has been contrasted with the exact solution for Eq. (27), and no noticeable differences were found.

To simulate the case in which we use the setup of Fig. 5 for breast characterization, we assume that the parameters of one of the media—namely, the resin layer—are known, and we must therefore fit the values of the intralipid. For the fitting functions, we shall use two cases, namely, a two-layered medium [Eq. (34)] and a one-layered medium. The expression for the one-layered medium is obtained by considering that parameters of the resin (see Fig. 5) are the same as the intralipid, and therefore

$$\tilde{U}_{\text{1layer}}(\mathbf{K}, z_d) = \frac{S_0}{4\pi^2 D_0} \frac{\exp[iq_0(\mathbf{K})(L_0 + L_1)]}{q_0(\mathbf{K})} \times \sinh[iq_0(\mathbf{K})z_s] \mathcal{T}_{\text{nd}}(\mathbf{K}), \quad (35)$$

where \mathcal{T}_{nd} is the transmission coefficient for the intralipid–air interface. For both the two-layer and one-layer expressions we shall use $z_s = l_{\text{tr}} = 3D_0 = 1/\mu_{s0}^{(i)}$.

To fit for $\mu_{a0}^{(j=1,\dots,5)}$ and $\mu_{s0}^{(i=1,2,3)}$, we first perform the two-dimensional Fourier transform $\tilde{U}_{\text{data}}^{(i,j)}(\mathbf{K})$ of the CCD measurements $U_{\text{data}}^{(i,j)}(\mathbf{R})$ corresponding to the $(\mu_{s0}^{(i)}, \mu_{a0}^{(j)})$ pair. We shall use a cutoff frequency $\mathbf{K}_{\text{cut}} = 1.2 \text{ cm}^{-1}$ to separate noise from the data. Then we normalize all $[\mu_{s0}^{(i=1,2,3)}, \mu_{a0}^{(j=1,\dots,5)}]$ sets to the value corresponding to $[\mu_{s0}^{(i=1)} = 5 \text{ cm}^{-1}, \mu_{a0}^{(j=1)} = 0.025 \text{ cm}^{-1}]$ at $\mathbf{K} = 0$, finally fitting for both $\mu_{s0}^{(i=1,2,3)}$ and $\mu_{a0}^{(j=1,\dots,5)}$. In this way, we make the assumption that we only have one reference measurement for which the values μ_{s0} and μ_{a0} are known. In all cases, the only restriction that we impose is that each set $\mu_{a0}^{(j=1,\dots,5)}$ is associated with the same

value of $\mu_{s0}^{(i)}$. The fitting procedure employed is the steepest-descent method, in which we shall always use $\mu_{a0} = 0.1 \text{ cm}^{-1}$, $\mu_{s0} = 3.33 \text{ cm}^{-1}$ as initial values (see Ref. 17 for comparison between different fitting procedures). The function to minimize is

$$f[\mu_{s0}^{(i)}, \mu_{a0}^{(j=1,\dots,5)}] = \sum_{\mathbf{K}} \|\bar{U}_{\text{theory}}^{(i,j=1,\dots,5)}(\mathbf{K}) - \bar{U}_{\text{data}}^{(i,j=1,\dots,5)}(\mathbf{K})\|^2, \quad (36)$$

where the subindex theory stands for either 2 layer or 1 layer [see Eqs. (34) and (35)], depending on the expression used to fit, and $\bar{U}_{\text{theory}}^{(i,j=1,\dots,5)}$ represent the expressions for the set $[\mu_{s0}^{(i)}, \mu_{a0}^{(j=1,\dots,5)}]$ normalized to the $\mathbf{K} = 0$ value corresponding to $(\mu_{s0} = 5 \text{ cm}^{-1}, \mu_{a0} = 0.025 \text{ cm}^{-1})$. To

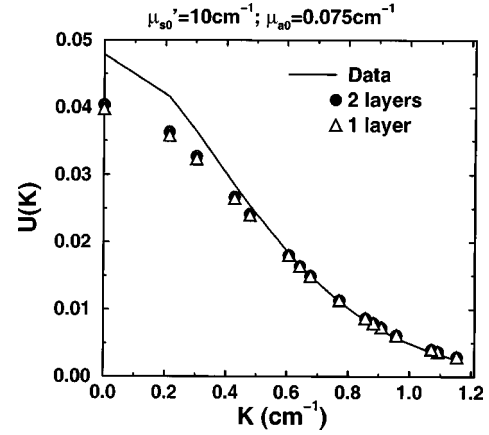


Fig. 6. Fitted values of $\bar{U}_{2\text{slab}}(\mathbf{K})$ (solid circles) and $\bar{U}_{1\text{slab}}(\mathbf{K})$ (open triangles), compared with the data values $\bar{U}_{\text{data}}(\mathbf{K})$ (solid curve) versus the frequency \mathbf{K} , for the case $\mu_{s0}' = 10 \text{ cm}^{-1}$, $\mu_{a0} = 0.075 \text{ cm}^{-1}$. See Eqs. (34) and (35).

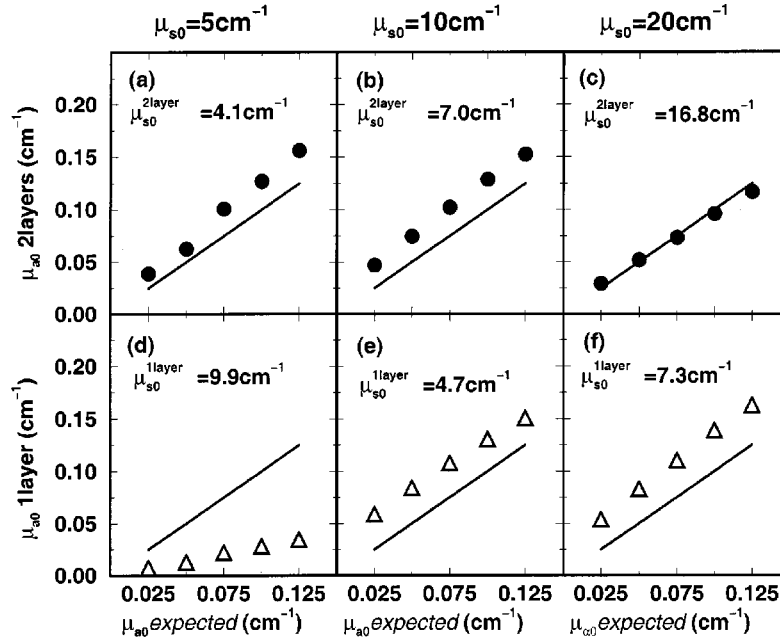


Fig. 7. Fitted values with use of the two-layer expression [Eq. (34)]: (a) $\mu_{s0}' = 5 \text{ cm}^{-1}$, (b) $\mu_{s0}' = 10 \text{ cm}^{-1}$, (c) $\mu_{s0}' = 20 \text{ cm}^{-1}$, and the one-layer expression [Eq. (35)]: (d) $\mu_{s0}' = 5 \text{ cm}^{-1}$, (e) $\mu_{s0}' = 10 \text{ cm}^{-1}$, (f) $\mu_{s0}' = 20 \text{ cm}^{-1}$. Symbols and solid curves, the expected and the retrieved values, respectively.

define the accuracy of each expression of retrieving the parameters, we define the average error for the retrieval of μ_{a0} in units of cm^{-1} as

$$\overline{\Delta\mu_{a0}} = \frac{1}{5} \sum_{j=1}^5 |\mu_{a0}^{\text{found}}(j) - \mu_{a0}^{\text{expected}}(j)| \quad [\text{cm}^{-1}], \quad (37)$$

where $\mu_{a0}^{\text{expected}}(j = 1\dots 5) = (0.025 \text{ cm}^{-1}, \dots, 0.125 \text{ cm}^{-1})$ are the expected values of μ_{a0} , and $\mu_{a0}^{\text{found}}(j = 1\dots 5)$ are those fitted from Eqs. (34) and (35).

6. RESULTS AND DISCUSSION

Figure 6 shows the fitted curves of $\bar{U}_{2\text{layer}}$ and $\bar{U}_{1\text{layer}}$ versus the frequency \mathbf{K} , contrasted with the data set \bar{U}_{data} for the case ($\mu'_{s0} = 10 \text{ cm}^{-1}$, $\mu_{a0} = 0.075 \text{ cm}^{-1}$). As shown, both expressions $\bar{U}_{2\text{layer}}$ and $\bar{U}_{1\text{layer}}$ yield close fits to the experimental data \bar{U}_{data} , even at high values of the frequency $\mathbf{K} \approx 1.2 \text{ cm}^{-1}$. However, as will be seen in the reconstructions, the values of (μ_{s0}^{found} , μ_{a0}^{found}), which yield the curves in Fig. 6 with use of the one-layer expression, Eq. (35), are far from the expected values but are very near the expected values when using the two-layer expression, Eq. (34). The results obtained from the fitting procedure are presented in Fig. 7 and Table 1, which show that the values of both $\mu_{s0}^{(i)}$ and $\mu_{a0}^{(j)}$ are retrieved with remarkable accuracy with the two-layer expression. On the other hand, the one-layer expression yields acceptable reconstruction values for $\mu_{a0}^{(j)}$ [see Figs. 7(d)–7(f)] but fails to reconstruct $\mu_{s0}^{(i)}$ (see Table 1). We would like to draw attention to the values of $\overline{\Delta\mu_{a0}}$ shown in Table 1. In this table, we show that the error of retrieval of μ_{a0} can amount to as high as $\pm 0.025 \text{ cm}^{-1}$ for the two-layer expression. If we look at Fig. 7(b), which shows the retrieved values of μ_{s0}^{found} versus the expected values of $\mu_{s0}^{\text{expected}}$, we see that even in the case in which $\overline{\Delta\mu_{a0}} = \pm 0.025 \text{ cm}^{-1}$ (which corresponds to $\mu_{s0} = 10 \text{ cm}^{-1}$), the relative values of $\mu_{s0}^{(j)}$ are correct. That is, if the exact value of one of them is known, then all the others lie correctly in place, yielding a very small value of $\overline{\Delta\mu_{a0}}$. Also, as shown in Table 1, the retrieved values of μ_{s0} are all within a 30% error for the two-layer expression, whereas for the one-layer expression they can be as high as 70%. The same calculations were performed with the expression for the semi-infinite configuration, Eq. (19), and in all cases the values of $\overline{\Delta\mu_{a0}}$ were of the order of $\pm 0.04 \text{ cm}^{-1}$, and the errors of retrieval for μ'_{s0} were $\sim 70\%$. We emphasize that when performing transmission measurements in the cw regime, in most cases the values of μ'_{s0} and μ_{a0} cannot be retrieved simultaneously from independent measurements unless we choose initial fitting values very close to the real ones. This is due to uncertainties in the measurements and in the optical properties, resulting in a large number of local minima that occur whenever the coefficients D_0 and μ_{a0} have the same relative values, i.e., $D_0^{\text{found}}/\mu_{a0}^{\text{found}} = D_0^{\text{expected}}/\mu_{a0}^{\text{expected}}$. Even so, we have been able to retrieve both values from independent measurements for the case with $\mu'_{s0} = 5 \text{ cm}^{-1}$ with errors lower than 15%, but we have found deviations in the order of 100% for the $\mu'_{s0} = 10 \text{ cm}^{-1}$, 20 cm^{-1} cases. Since results were not

Table 1. Comparison of the Fitted Values Obtained with Eqs. (34) and (35), Two-Layered Medium and One-Layered Medium, Respectively^a

$\mu_{s0}^{\text{expected}}$ (cm^{-1})	$\mu_{s0}^{2\text{layer}}$ (cm^{-1})	$\overline{\Delta\mu_{a0}^{2\text{layer}}}$ (cm^{-1})	$\mu_{s0}^{1\text{layer}}$ (cm^{-1})	$\overline{\Delta\mu_{a0}^{1\text{layer}}}$ (cm^{-1})
5.0	4.1	± 0.022	9.9	± 0.059
10.0	7.0	± 0.025	4.7	± 0.032
20.0	16.8	± 0.004	7.3	± 0.035

^a $\mu_{s0}^{2\text{layer}}$ are the fitted values for μ_{s0} using the two-layer and one-layer expressions, respectively, and $\overline{\Delta\mu_{a0}^{2\text{layer}}}$ is the average error of retrieval of μ_{a0} , Eq. (37).

general, independent fits are not presented. As shown in Refs. 17 and 18 this does not occur when measuring spatially resolved reflection in the cw regime. Also, when performing reflection measurements in the frequency or time domains, it has been shown experimentally that one can also fit for the slab width L_0 with great accuracy, but that fitting for all the optical parameters of both resin and intralipid yields errors higher than 200% (Ref. 23).

7. CONCLUSIONS

We have put forward the expressions for the reflection and transmission coefficients at diffusive–nondiffusive interfaces. These coefficients, together with those already established for diffusive–diffusive interfaces,²⁴ can be used to find the exact solution for any multiple-layered configuration, in either the time domain or the frequency domain, and hence to retrieve the optical parameters. In addition to being useful in characterizing multiple-layered media or in finding the exact solution of complex forward problems, these coefficients also constitute a powerful tool to generate more-accurate Green's functions that can be used to detect and characterize hidden objects within such media.^{8,40,41} With these expressions we have shown that any multiple-layered system can be rigorously solved at a very low computational cost. We have put forward the simple example of a slab for which the reflection and transmission coefficients have been derived. The expressions for a slab can be used to obtain the limiting distance at which multiple reflections between two interfaces exist and also to give information about using reflection measurements to characterize objects buried at a certain distance under an interface. A comparison with a dielectric slab has been presented, demonstrating that in the case of diffusive waves no interference resonant peaks can be observed and therefore that interferometers based on plane parallel plates, such as the Fabry–Perot, cannot be operated for diffusive waves. The expression for a slab is also useful, since in most cases multiple-layered media can be approximated to a series of slabs with no multiple reflections between them.

Once we have established the method for solving multiple-layered media, we have characterized a two-layered system from experimental data for 15 different (μ'_s , μ_a) pairs. In this characterization procedure we have demonstrated that using the expression for a two-layered system yields better reconstructed values for both μ'_s and μ_a than the one-layer, or semi-infinite expression.

We have shown that by means of the two-layer expression obtained from the reflection and transmission coefficients, we can reconstruct both the values of μ'_s and μ_a from transmission measurements without any *a priori* information on their values by using one reference measurement. In all cases the values of μ'_s and μ_a were retrieved within a $\sim 30\%$ error.

ACKNOWLEDGMENTS

We thank an anonymous reviewer for valuable comments. This research has been partially supported by the Fundación Ramón Areces. J. Ripoll acknowledges a grant from the Ministerio de Educación y Cultura. V. Ntziachristos acknowledges National Institutes of Health grant CA60182. A Fortran program for solving exactly any M -layered system is available on request at jripoll@iesl.forth.gr.

Corresponding author J. Ripoll can be reached at Institute of Electronic Structure and Laser, FORTH, P.O. Box 1527, GR-71110 Heraklion, Greece, or by e-mail at jripoll@iesl.forth.gr.

REFERENCES AND NOTES

1. A. Ishimaru, *Wave Propagation and Scattering in Random Media* (Academic, New York, 1978), Vol. 1.
2. M. S. Patterson, B. Chance, and B. C. Wilson, "Time-resolved reflectance and transmittance for the noninvasive measurement of tissue optical properties," *Appl. Opt.* **28**, 2331–2336 (1989).
3. A. Yodh and B. Chance, "Spectroscopy and imaging with diffusing light," *Phys. Today* **48**, 38–40 (1995).
4. H. Jiang, K. D. Paulsen, U. L. Osterberg, B. W. Pogue, and M. S. Patterson, "Simultaneous reconstruction of optical absorption and scattering maps in turbid media from near-infrared frequency-domain data," *Opt. Lett.* **20**, 2128–2130 (1995).
5. S. R. Arridge, P. Van Der Zee, M. Cope, and D. T. Delpy, "Reconstruction methods for near-infrared absorption imaging," in *Time-Resolved Spectroscopy and Imaging of Tissues*, B. Chance and A. Katzir, eds., *Proc. SPIE* **1431**, 204–215 (1991).
6. E. B. de Haller, "Time-resolved transillumination and optical tomography," *J. Biomed. Opt.* **1**, 7–17 (1996).
7. S. Fantini, S. A. Walker, M. A. Franceschini, M. Kaschke, P. M. Schlag, and K. T. Moesta, "Assessment of the size, position, and optical properties of breast tumors *in vivo* by noninvasive optical methods," *Appl. Opt.* **37**, 1982–1989 (1998).
8. V. Ntziachristos, X. Ma, and B. Chance, "Time-correlated single photon counting imager for simultaneous magnetic resonance and near-infrared mammography," *Rev. Sci. Instrum.* **69**, 4221–4233 (1998).
9. S. R. Arridge, "Optical tomography in medical imaging," *Inverse Probl.* **15**, R41–R93 (1999).
10. J. G. Fujimoto and M. S. Patterson, eds., *Advances in Optical Imaging and Photon Migration*, Vol. 21 of OSA Trends in Optics and Photonic Series (Optical Society of America, Washington, D.C., 1998).
11. M. A. O'Leary, D. A. Boas, B. Chance, and A. G. Yodh, "Refraction of diffuse photon density waves," *Phys. Rev. Lett.* **69**, 2658–2661 (1992).
12. J. B. Frishkin and E. Gratton, "Propagation of photon-density waves in strongly scattering media containing an absorbing semi-infinite plane bounded by a straight edge," *J. Opt. Soc. Am. A* **10**, 127–140 (1993).
13. M. Keijzer, W. M. Star, and P. R. M. Storchi, "Optical diffusion in layered media," *Appl. Opt.* **27**, 1820–1824 (1988).
14. J. M. Schmitt, G. X. Zhou, and E. C. Walker, "Multilayer model of photon diffusion in skin," *J. Opt. Soc. Am. A* **7**, 2141–2153 (1990).
15. I. Dayan, S. Havlin, and G. H. Weiss, "Photon migration in a two-layer turbid medium: a diffusion analysis," *J. Mod. Opt.* **39**, 1567–1582 (1992).
16. A. H. Hielscher, H. Liu, and B. Chance, "Time-resolved photon emission from layered turbid media," *Appl. Opt.* **35**, 2221–2227 (1996).
17. G. Alexandrakis, T. J. Farrell, and M. S. Patterson, "Accuracy of the diffusion approximation in determining the optical properties of a two-layer turbid medium," *Appl. Opt.* **37**, 7401–7409 (1998).
18. T. J. Farrell, M. S. Patterson, and M. Essenpreis, "Influence of layered tissue architecture on estimates of tissue optical properties obtained from spatially resolved diffuse reflectometry," *Appl. Opt.* **37**, 1958–1972 (1998).
19. A. Kienle, M. S. Patterson, N. Dögnitz, "Noninvasive determination of the optical properties of two-layered turbid media," *Appl. Opt.* **37**, 779–791 (1998).
20. A. Kienle, T. Glanzmann, G. Wagnieres, "Investigation of two-layered turbid media with time-resolved reflectance," *Appl. Opt.* **37**, 6852–6862 (1998).
21. L. O. Svaasand, T. Spott, J. B. Frishkin, T. Pham, B. J. Tromberg, and M. W. Berns, "Reflectance measurements of layered media with diffuse photon-density waves: a potential tool for evaluating deep burns and subcutaneous lesions," *Phys. Med. Biol.* **44**, 801–813 (1999).
22. G. Alexandrakis, T. J. Farrell, and M. S. Patterson, "Monte Carlo diffusion hybrid model for photon migration in a two-layer turbid medium in the frequency domain," *Appl. Opt.* **39**, 2235–2244 (2000).
23. T. H. Pham, T. Spott, L. O. Svaasand, and B. J. Tromberg, "Quantifying the properties of two-layer turbid media with frequency-domain diffuse reflectance," *Appl. Opt.* **39**, 4733–4745 (2000).
24. J. Ripoll and M. Nieto-Vesperinas, "Reflection and transmission coefficients for diffuse photon-density waves," *Opt. Lett.* **24**, 796–798 (1999).
25. M. Born and E. Wolf, *Principles of Optics*, 6th ed. (Pergamon, New York, 1993).
26. J. W. Goodman, *Introduction to Fourier Optics* (McGraw-Hill, New York, 1968).
27. L. Mandel and E. Wolf, *Optical Coherence and Quantum Optics* (Cambridge U. Press, Cambridge UK, 1995).
28. M. Nieto-Vesperinas, *Scattering and Diffraction in Physical Optics* (Wiley-Interscience, New York, 1991).
29. J. Ripoll, M. Nieto-Vesperinas, and R. Carminati, "Spatial resolution of diffuse photon density waves," *J. Opt. Soc. Am. A* **16**, 1466–1476 (1999).
30. J. Ripoll, S. R. Arridge, H. Dehghani, and M. Nieto-Vesperinas, "Boundary conditions for light propagation in diffusive media with nonscattering regions," *J. Opt. Soc. Am. A* **17**, 1671–1681 (2000).
31. R. C. Haskell, L. O. Svaasand, T. Tsay, T. Feng, M. S. McAdams, and B. J. Tromberg, "Boundary conditions for the diffusion equation in radiative transfer," *J. Opt. Soc. Am. A* **11**, 2727–2741 (1994).
32. R. Aronson, "Boundary conditions for diffusion of light," *J. Opt. Soc. Am. A* **12**, 2532–2539 (1995).
33. A. Banos, *Dipole Radiation in the Presence of a Conducting Half-Space* (Pergamon, New York, 1966).
34. X. De Li, T. Durduran, A. G. Yodh, B. Chance, and D. N. Pattanayak, "Diffraction tomography for biochemical imaging with diffuse-photon density waves," *Opt. Lett.* **22**, 573–575 (1997).
35. T. Durduran, J. P. Culver, M. J. Holboke, X. D. Li, L. Zubkov, B. Chance, D. N. Pattanayak, and A. G. Yodh, "Algorithms for 3D localization and imaging using near-field diffraction tomography with diffuse light," *Opt. Exp.* **4**, 247–262 (1999).
36. D. N. Pattanayak and A. G. Yodh, "Diffuse optical 3D-slice imaging of bounded turbid media using a new integrodifferential equation," *Opt. Exp.* **4**, 231–240 (1999).
37. A. Yariv, *Introduction to Optical Electronics*, 2nd ed. (Holt, Rinehart & Winston, New York, 1976).
38. J. Ripoll and M. Nieto-Vesperinas, "Index mismatch for dif-

- fuse photon-density waves both at flat and rough diffuse-diffuse interfaces," *J. Opt. Soc. Am. A* **16**, 1947–1957 (1999).
39. Detailed information on the components and on how to build the resin can be found at <http://www.med.upenn.edu/~oisg/oisg.html>.
 40. V. Ntziachristos, X. Ma, A. G. Yodh, and B. Chance, "Multichannel photon counting instrument for spatially resolved near-infrared spectroscopy," *Rev. Sci. Instrum.* **70**, 193–201 (1999).
 41. V. Ntziachristos, B. Chance, and A. G. Yodh, "Differential diffuse optical tomography," *Opt. Exp.* **5**, 230–242 (1999).